Atmospheric
Chemistry
and Physics

Open Access

EGU

Supplement of

Sulfuric acid–amine nucleation in urban Beijing

Runlong Cai et al.

Correspondence to: Jingkun Jiang (jiangjk@tsinghua.edu.cn)

Simplified kinetic model

The schematic diagram of the simplified kinetic model is shown in Fig. S1. The reactions included in this model are as follows:

$$A + B \ \rightarrow \ A_1B_1 \qquad\qquad k_1 = \beta_{AB} \qquad (S1)$$

$$A_1B_1 \ \rightarrow \ A + B \qquad\qquad k_2 = \gamma_1 \qquad (S2)$$

$$A_1B_1 + A \ \rightarrow \ A_2B_1 \qquad\qquad k_3 = \beta_{1A} \qquad (S3)$$

$$2A_1B_1 \ \rightarrow \ A_2B_2 \qquad\qquad k_4 = 0.5\beta_{11} \qquad (S4)$$

$$A_2B_1 + B \ \rightarrow \ A_2B_2 \qquad\qquad k_5 = \beta_{2B} \qquad (S5)$$

$$A_2B_2 + A_1B_1 \ \rightarrow \ A_3B_3 \qquad\qquad k_6 = \beta_{21} \qquad (S6)$$

$$A_3B_3 + A_1B_1 \ \rightarrow \ A_4B_4 \qquad\qquad k_7 = \beta_{31} \qquad (S7)$$

$$A_4B_4 + A_1B_1 \ \rightarrow \ A_5B_5 \qquad\qquad k_8 = \beta_{41} \qquad (S8)$$

$$2A_2B_2 \ \rightarrow \ A_4B_4 \qquad\qquad k_9 = 0.5\beta_{22} \qquad (S9)$$

$$A_1B_1(g) \ \rightarrow \ A_1B_1(p) \qquad\qquad k_{10} = CS_1 \qquad (S10)$$

$$A_2B_1(g) \ \rightarrow \ A_2B_1(p) \qquad\qquad k_{11} = CS_{2'} \qquad (S11)$$

$$A_2B_2(g) \ \rightarrow \ A_2B_2(p) \qquad\qquad k_{12} = CS_2 \qquad (S12)$$

$$A_3B_3(g) \ \rightarrow \ A_3B_3(p) \qquad\qquad k_{13} = CS_3 \qquad (S13)$$

$$A_4B_4(g) \ \rightarrow \ A_4B_4(p) \qquad\qquad k_{14} = CS_4 \qquad (S14)$$
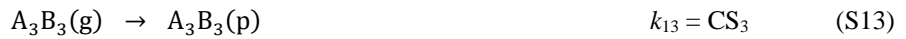
where A is H_2SO_4, B is dimethylamine (DMA) or trimethylamine (TMA), (g) represents the gas phase, (p) the represents particle phase, k_x is the reaction rate and x is the equation number, β is the collision coefficient, γ is the evaporation rate, and CS is the condensation sink. The subscripts of β, γ, and CS indicate their corresponding equations. The enhancement of coagulation due to van der Waals forces is considered for β and CS. The Hamaker constant is assumed to be 6.4×10^{-20} J. The enhancement factor for the coagulation between molecules or clusters was estimated to be 2.3, and it was estimated to be 1.3 for CS (Chan and Mozurkewich, 2001; Kürten et al., 2018; Stolzenburg et al., 2019). The correction factor of 2.3 agrees with the results obtained by atomistic simulation (Halonen et al., 2019).

The concentrations of $A_{1,tot}$, B, CS, and the ambient temperature are used as the input of this model. $A_{1,tot}$ refers to all the sulfuric acid monomers regardless of their base number. CS was calculated using the measured aerosol size distributions and the sticking probability for every collision between a particle and a cluster is assumed to be 100 %. The value of CS varies with clusters because of their varying diameters (Lehtinen et al., 2007). The value of γ was calculated according to the theoretical standard molar Gibbs free energy of reaction obtained by quantum chemistry calculation (Ortega et al., 2012). The influence of temperature on γ is accounted for using the following formula:

$$\frac{\Delta_f G_m^\theta(T_1)}{T_1} \ = \ \frac{\Delta_f G_m^\theta(T_0)}{T_0} - \int_{T_0}^{T_1} \frac{\Delta_f H_m^\theta}{T^2} dT \qquad (S15)$$

where $\Delta_f G_m^\theta$ is the standard molar Gibbs free energy of formation (of A_1B_1), T_1 is the targeted temperature, $T_0 = 298.15$ K, $\Delta_f H_m^\theta$ is the standard molar enthalpy of formation.

The $\Delta_f G_{m,A1B1}^\theta$ is assumed to be -14.0 kcal/mol, which is higher than the value of -13.5 kcal/mol reported in Myllys et al.

39 (2019) but lower than the values of -14.4 and -15.4 kcal/mol reported in Ortega et al. (2012). This value was chosen to fit the

40 measured H_2SO_4 dimer concentration and particle formation rate of 1.4 nm particles. Due to the measurement uncertainties,

41 it is difficult to conclude that -14.0 kcal/mol is more accurate than -13.5 or -14.4 kcal/mol for $\Delta_f G_{m,A1B1}^{\theta}$, yet we use -14.0

42 kcal/mol for its better accordance with the measurements.

43 Considering the fast conversion between A and A_1B_1, Eqs. S1 and S2 are assumed to be at a quasi-steady state. Hence, the

44 concentrations of A and A_1B_1 were calculated using Eq. 1. For A_2B_1, A_2B_2, A_3B_3, and A_4B_4, their concentration change rates

45 derived from Eq. S3-S14 are shown in Eq. S16-S20 and their concentrations are solved numerically in the simplified kinetic

46 model.

$$\frac{d[A_1B_1]}{dt} = k_1[A][B] - k_2[A_1B_1] - k_3[A_1B_1][A] - 2k_4[A_1B_1]^2 - k_6[A_2B_2][A_1B_1] - k_7[A_3B_3][A_1B_1]$$
$$- -k_8[A_4B_4][A_1B_1] - k_{10}[A_1B_1] \tag{S16}$$

$$\frac{d[A_2B_1]}{dt} = k_3[A_1B_1][A] - k_5[A_2B_1][B] - k_{11}[A_2B_1] \tag{S17}$$

$$\frac{d[A_2B_2]}{dt} = k_4[A_1B_1]^2 + k_5[A_2B_1][B] - k_6[A_2B_2][A_1B_1] - 2k_9[A_2B_2]^2 - k_{12}[A_2B_2] \tag{S18}$$

$$\frac{d[A_3B_3]}{dt} = k_6[A_2B_2][A_1B_1] - k_7[A_3B_3][A_1B_1] - k_{13}[A_3B_3] \tag{S19}$$

$$\frac{d[A_4B_4]}{dt} = k_7[A_3B_3][A_1B_1] + k_9[A_2B_2]^2 - k_8[A_4B_4][A_1B_1] - k_{14}[A_4B_4] \tag{S20}$$

47 The formation rate of A_4B_4 is taken as the simulated particle formation rate, J_{A4B4}, and it was calculated using Eq. S21. Note

48 that according to this simulation, during the campaign in urban Beijing, the clustering of A_2B_2 contributes only a minor

49 proportion to J_{A4B4}.

$$J_{A4B4} = k_7[A_3B_3][A_1B_1] + k_9[A_2B_2]^2 \tag{S21}$$

50

51 **Derivation of equations 1 and 2 in the main text**

52 Although J_{A4B4} is numerically solved in the simplified model, an illustrative analytical solution based on a series of

53 approximations for J_{A4B4} is given below for a better understanding of Eqs. 1 and 2 in the main text. Putting the time derivative

54 terms on the left-hand sides of Eqs. S16-S20 to zero yields the following steady-state concentrations of these H_2SO_4-amine

55 clusters:

$$[A_1B_1] = \frac{k_1[A][B]}{k_2 + k_3[A] + 2k_4[A_1B_1] + k_6[A_2B_2] + k_7[A_3B_3] + k_8[A_4B_4] + k_{10}} \approx \frac{k_1[A][B]}{k_2 + k_{10}} \tag{S22}$$

$$[A_2B_1] = \frac{k_3[A_1B_1][A]}{k_5[B]+k_{11}} \tag{S23}$$

$$[A_2B_2] = \frac{k_4[A_1B_1]^2 + k_5[A_2B_1][B]}{k_6[A_1B_1] + 2k_9[A_2B_2] + k_{12}} \approx \frac{k_4[A_1B_1]^2 + k_5[A_2B_1][B]}{k_{12}} \tag{S24}$$

$$[A_3B_3] = \frac{k_6[A_2B_2][A_1B_1]}{k_7[A_1B_1] + k_{13}} \approx \frac{k_6[A_2B_2][A_1B_1]}{k_{13}} \tag{S25}$$

$$[A_4B_4] \; = \; \frac{k_7[A_3B_3][A_1B_1] + k_9[A_2B_2]^2}{k_8[A_1B_1] + k_{14}} \approx \frac{k_7[A_3B_3][A_1B_1] + k_9[A_2B_2]^2}{k_{14}} \tag{S26}$$

56 Due to the comparatively high CS in urban Beijing, the cluster growth rates are usually much smaller than their loss rates.
57 As a result, the solution for the steady-state concentrations of H$_2$SO$_4$-amine clusters can be simplified as above. Such
58 simplifications are reasonable for the ambient conditions during this campaign (indicated by the horizontal coordinate in Fig.
59 4).

60 Since the concentrations of A and A$_1$B$_1$ are assumed to be at the steady-state and the sum of their concentrations is equal to
61 the concentration of A$_{1,\text{tot}}$, the relationship between the concentrations of A$_{1,\text{tot}}$ and A$_1$B$_1$ can be readily obtained according to
62 Eq. S22:

$$\frac{[A_1B_1]}{[A_{\text{tot}}]} \; \approx \; \frac{k_1[B]}{k_2 + k_{10} + k_1[B]} \; = \; \frac{\beta_{\text{AB}}[B]}{\gamma_1 + CS_1 + \beta_{\text{AB}}[B]} \; := \; \eta \tag{S27}$$

63 Combining Eq. S22-S25, the simplified analytical solution for J_{A4B4} is:

$$
\begin{aligned}
J_{\text{A4B4}} \; = \; & \frac{k_4 k_6 k_7}{k_{12} k_{13}}\big[A_{1,\text{tot}}\big]^4 \eta^4 \left[1 + \frac{k_3}{k_4}\frac{(1-\eta)}{\eta}\frac{k_5[B]}{(k_5[B]+k_{11})}\right] \\
& + \frac{k_4{}^2 k_9}{k_{12}{}^2}\big[A_{1,\text{tot}}\big]^4 \eta^4 \left[1 + \frac{k_3}{k_4}\frac{(1-\eta)}{\eta}\frac{k_5[B]}{(k_5[B]+k_{11})}\right]^2
\end{aligned}
\tag{S28}
$$

64

Considerations on the simplifications of the model

66 This kinetic model is proposed based on both the measured data and the quantum chemistry calculation. The growth of
67 clusters and particles in an H$_2$SO$_4$-amine system is driven by the clustering of H$_2$SO$_4$ and amine molecules. The detailed
68 growth pathway is determined by the evaporation rate of each A$_n$B$_m$ cluster and their concentrations. The evaporation and
69 fission rates of each cluster can be estimated according to quantum chemistry calculation and the reaction pathway under a
70 given condition can thus be derived (McGrath et al., 2012). However, due to the uncertainties in the quantum chemistry
71 calculation, the evaporation rates estimated using different levels of theory deviates from each other in order of magnitudes.
72 For instance, at 298.15 K, the evaporation rate of (H$_2$SO$_4$)$_1$(amine)$_1$ in Ortega et al. (2012) and Myllys et al. (2019) was
73 estimated to be 0.14 s^{-1} and 3.1 s^{-1} (after correcting the influence of van der Waals force), respectively. Note that the
74 uncertainties in the evaporation rates of larger clusters are perhaps higher because they contain more atoms than A$_1$B$_1$ does.
75 Meanwhile, it is difficult to determine the base number of a neutral H$_2$SO$_4$-amine cluster using the mass spectrometer (ToF-
76 CIMS) because amine may detach from the H$_2$SO$_4$-amine cluster due to ionization, evaporation, and fragmentation during
77 the detection.

78 As a result, we include only A$_n$B$_n$ (n = 1, 2, 3, 4) and A$_2$B$_1$ clusters in the simplified model. Considering measurement
79 uncertainties, the simulated results using this simplified model were found to agree with the measured data (Figs. 1, 2, and
80 3). The stability of A$_2$B$_1$ is supported by both the quantum chemistry results(Ortega et al., 2012; Myllys et al., 2019). The
81 estimated relative stability of A$_{n-1}$B$_n$ (n = 3, 4) under the ambient conditions is still not clear due to the uncertainties of
82 quantum chemistry calculation. For instance, the total evaporation (including monomer evaporation and fission) rates of A$_3$B$_2$
83 were estimated to be 8.3 s^{-1} and 0.6 s^{-1} at 298.15 K in Ortega et al. (2012) and Myllys et al. (2019), respectively. These values
84 indicate that A$_3$B$_2$ is perhaps unstable or semi-stable in the ambient conditions. Due to the measurement uncertainties, it is
85 difficult to estimate the contribution of A$_3$B$_2$ contribution to total H$_2$SO$_4$ trimer concentration by comparing the measured

86   data and simulation results. Hence, $A_{n-1}B_n$ (n = 3, 4) are not included in the simplified model. Other A_nB_m clusters in addition

87   to A_nB_n and $A_{n-1}B_n$ are much more unstable compared to A_nB_n, e.g., the evaporation rate of A_3B_1 was estimated to be 8.5 s^{-1}

88   and 103 s^{-1} at 298.15 K in Ortega et al. (2012) and Myllys et al. (2019), respectively.

89   As mentioned in the above section and the main text, the depletion of an H_2SO_4- amine cluster due to its growth is neglected

90   in Eqs. 1 and S22 – S26. We use the example of A_1B_1 to show that this approximation is reasonable in the polluted

91   atmospheric boundary layer. Note that this approximation is used when deriving Eq. 1 but not in the model. Under the typical

92   condition in this field campaign, e.g., $[A_{1,tot}] = 5 \times 10^6$ cm^{-3}, CS = 1.7×10^{-2} s^{-1}, DMA = 1.8 ppt, T = 281 K, and the values of

93    $k_3[A]$ and $2k_4[A_1B_1]$ in Eq. S22 are approximately 4.2×10^{-3} s^{-1} and 2.0×10^{-3} s^{-1}, respectively. These values are an order of

94   magnitude smaller than k_2 (γ_1 = 0.11 s^{-1}) and k_{10} (CS = 1.7×10^{-2} s^{-1}). The concentrations of H_2SO_4 trimer and tetramer are

95   orders of magnitudes lower than H_2SO_4 dimer concentrations in urban Beijing, hence, the values of $k_6[A_2B_2]$ and $k_7[A_3B_3]$

96   are even smaller compared to k_2 and k_{10}. This estimation is supported by the horizontal position of the measured data in Fig.

97   4. Similarly, the evaporation of some stable clusters, e.g., A_2B_2, is neglected because its value is orders of magnitudes smaller

98   than the CS in urban Beijing.

99

100   **Scaling of formation rate in Figure 3**

101   In Eqs. S28, k_4, k_6, k_7, and k_9 are (half of) the collision coefficients between clusters and they are proportional to β_{11}. k_{12} and

102   k_{13} are coagulation sinks and they are proportional to CS. The term $1 + k_3(1 - \eta)k_5[B]/[k_4\eta(k_5[B]+k_{11})]$ is dependent

103   on amine concentration and it approaches 1 when [B] increases. Hence, it can be approximated that the formation rate of

104   A_4B_4 clusters is proportional to $[A_{1,tot}]^4$ and CS^{-2}. Figures 3a and S7 below indicate that the power of $[A_{1,tot}]$ should 3.6 instead

105   of 4 for urban Beijing, yet this minor difference does not significantly affect the conclusions. The size of an A_4B_4 cluster (B

106   = DMA) was estimated to be ~1.4 nm (Thomas et al., 2016). Since $[A_{1,tot}]$ and CS are important factors determining the

107   formation rate, the measured $J_{1.4}$ has to be scaled with respect to them before comparison. For example, a scaling method for

108   CS is given below:

$$J_{1.4,\text{scaled}} = J_{1.4,\text{measured}} \frac{CS^2}{CS_{\text{ref}}{}^2} \tag{S29}$$

109   where $J_{1.4,\text{measured}}$ and $J_{1.4,\text{scaled}}$ are the measured and scaled formation rates of 1.4 nm particles, respectively; CS is the measured

110   condensation sink; CS_{ref} is the reference condensation sink and it is chosen as 0.017 s^{-1} in Fig. 1, which is a typical value (the

111   median value during NPF events) in urban Beijing during this campaign. The values of the scaled formation rates are mainly

112   affected by H_2SO_4 concentration and amine concentrations.

113

114   **Analytical solution for the model in clean environments**

115   The above discussion is based on the assumption of a high CS, and the approximate solution of J_{A4B4} is given in Eq. S28.

116   However, in clean environments with low CS, the sink for H_2SO_4-amine clusters is usually determined by their condensation

117   growth rather than the coagulation scavenging. Considering that the monomer concentration is much higher than the

118   concentrations of dimer and trimer, Eq. 22-25 is simplified to obtain an approximate analytical solution that applies for clean

119   environments:

$$[A_1B_1] \approx \frac{k_1[A][B]}{k_2 + k_3[A] + 2k_4[A_1B_1] + k_{10}} \tag{S30}$$

$$[A_2B_1] = \frac{k_3[A_1B_1][A]}{k_5[B]+k_{11}} \tag{S31}$$

$$[A_2B_2] = \frac{k_4[A_1B_1]^2 + k_5[A_2B_1][B]}{k_6[A_1B_1] + 2k_9[A_2B_2] + k_{12}} \tag{S32}$$

$$[A_3B_3] = \frac{k_6[A_2B_2][A_1B_1]}{k_7[A_1B_1] + k_{13}} \tag{S33}$$

120 The solutions for Eq. S32 and S34 are:

$$[A_1B_1] = \frac{\sqrt{\left(k_1[B] + k_2 + k_3[A_{1,tot}] + k_{10}\right)^2 + 4k_1(2k_4 - k_3)[A_{1,tot}][B]}}{4k_4 - 2k_3} \tag{S34A}$$
$$- \frac{k_1[B] + k_2 + k_3[A_{1,tot}] + k_{10}}{4k_4 - 2k_3}$$

$$\text{or } [A_1B_1] \approx \frac{k_1[B]}{k_1[B] + k_2 + k_3[A_{1,tot}] + k_{10}}[A_{1,tot}] \ (assuming \ k_3 = 2k_4) \tag{S34B}$$

$$[A] = [A_{1,tot}] - [A_1B_1] \tag{S35}$$

$$[A_2B_2] = \frac{\sqrt{(k_6[A_1B_1] + k_{12})^2 + 8k_9(k_4[A_1B_1]^2 + k_5[A_2B_1][B])}}{4k_9} - \frac{k_6[A_1B_1] + k_{12}}{4k_9} \tag{S36}$$

121 The expression for J_{A4B4} is:

$$J_{A4B4} = k_7[A_3B_3][A_1B_1] + k_9[A_2B_2]^2 \tag{S37}$$

122 The input for Eq. S37 are $[A_{1,tot}]$, $[B]$, and k_1-k_{13} which are mainly influenced by CS and T. $[A_1B_1]$, $[A]$, $[A_2B_1]$, $[A_2B_2]$, and
123 $[A_3B_3]$ are given in Eqs. S34, S35, S31, S36, and S33, respectively. The values of k_1-k_{13} are indicated in Eqs. S1-S13. Equation
124 S37 is more accurate than Eq. S28 because Eq. S37 does not neglect the sinks due to condensation growth. However, note
125 that Eq. S37 is derived base on a balance assumption. When the NPF period is shorter than the period for the clusters to reach
126 their steady-state concentrations, Eq. S37 will overestimate the formation rate.

Supporting figures
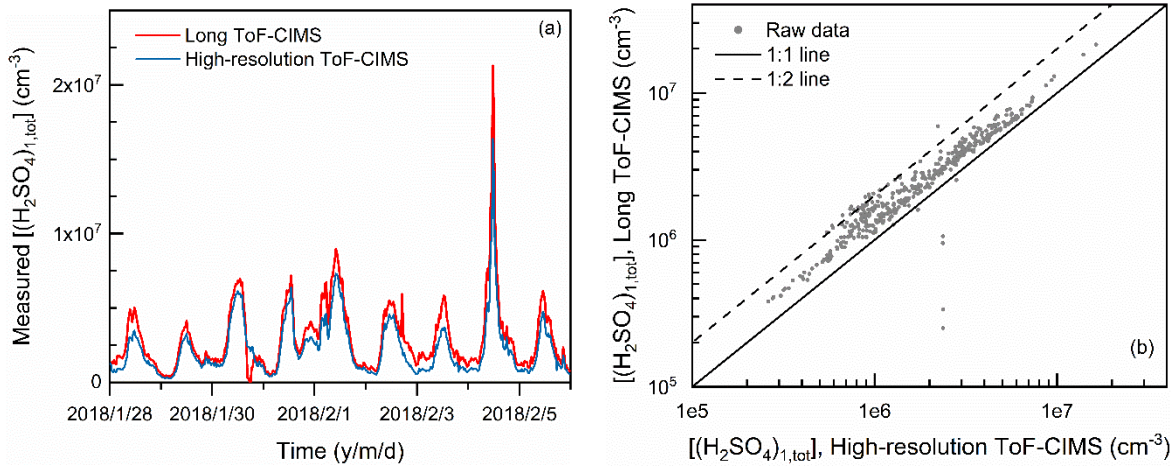
Figure S1: (a) Time series and (b) a scatter plot of the $(H_2SO_4)_{1,tot}$ concentration measured by a high-resolution ToF-CIMS and a long ToF-CIMS. The ratio of the $(H_2SO_4)_{1,tot}$ concentration measured by the long ToF-CIMS to that of the high-resolution ToF-CIMS is 1.4±0.3, where 0.3 is the standard deviation. According to (b), the uncertainty of the H_2SO_4 measured in this study was estimated to be 100%.
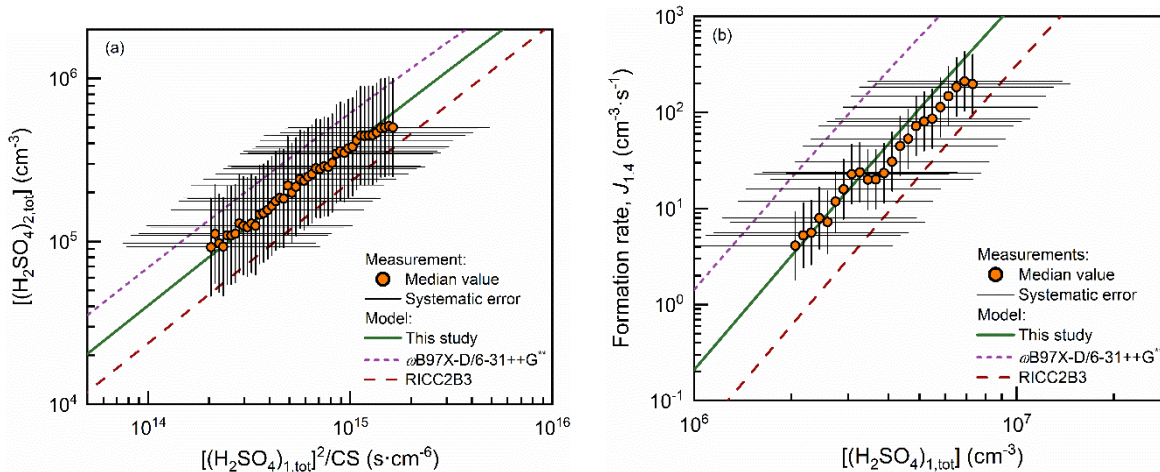
Figure S2: The potential systematic errors for (a) Fig. 1a. and (b) Fig. 1b. The error bar indicates the standard deviation of data due to systematic errors. The uncertainties of CS, $[(H_2SO_4)_{1,tot}]$, $[(H_2SO_4)_{2,tot}]$, and $J_{1.4}$ are detailed in the main text. The uncertainty of $[(H_2SO_4)_{1,tot}]^2/CS$ was estimated according to the formula for error propagation,

$$\sigma\left\{[(H_2SO_4)_{1,tot}]^2/CS\right\} = \sqrt{\left(2\sigma\{(H_2SO_4)_{1,tot}\}\right)^2 + (\sigma\{CS\})^2},$$

where σ indicates the relative error. The uncertainty range of simulation was estimated using the evaporation rate of $(H_2SO_4)_1(amine)_1$ from different literature (Ortega et al., 2012; Myllys et al., 2019). ωB97X-D/6-31++G** and RICC2B3 indicate the evaporation rates therein. The uncertainty in the amine measurement is included in the simulation, i.e., the higher simulation curve uses [amine]$\times$(1+σ_{amine}) as the model input while the low curve uses [amine]$\times$(1-σ_{amine}).
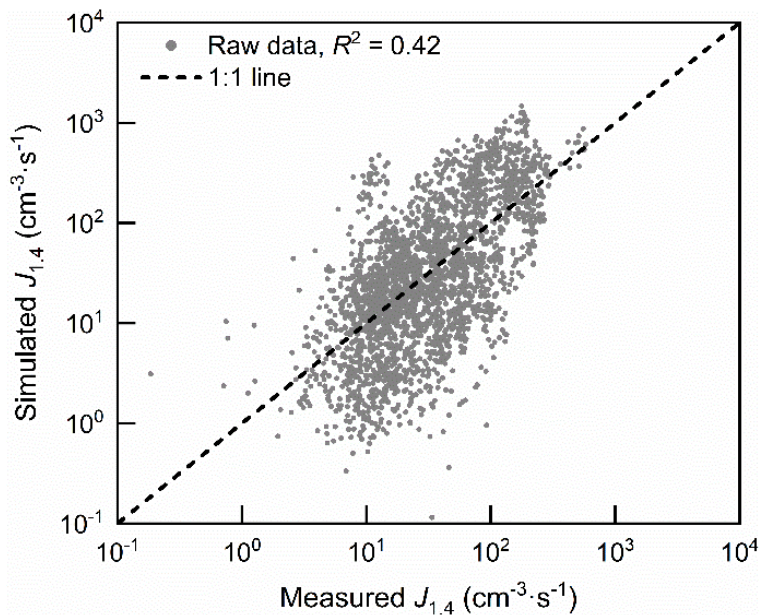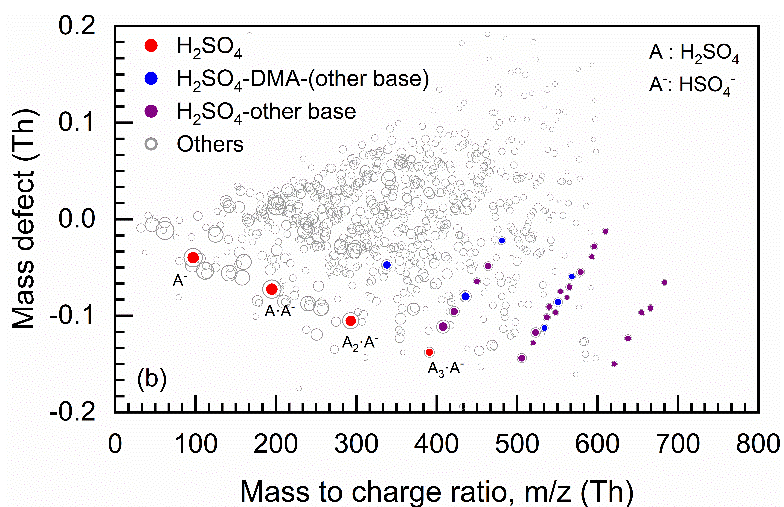
142

143 Figure S3: The correlation between the simulated and measured particle formation rates ($J_{1.4}$). The R^2 value was calculated
144 using logarithmic values. This figure uses the same dataset as Fig. 3b. The temporal resolution of the raw data is 5 min, which
145 is determined by the aerosol size spectrometers.
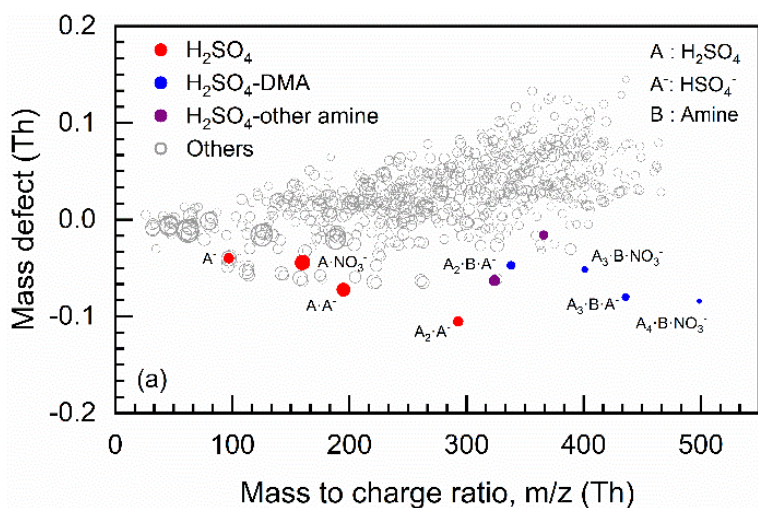
Figure S4: Mass defect plots of (a) neutral clusters measured by a ToF-CIMS and (b) naturally charged clusters measured by an Api-ToF-MS on Feb. 24, 2018. The dot size indicates the ion count number of each corresponding peak per unit volume. The ion counts were averaged between 11:30 and 12:30. The neutral clusters in (a) were charged using a nitrate source and only the chemical species after charging are shown. The red dots represent the measured H_2SO_4 clusters without amine, while the blue and purple dots represent H_2SO_4 clusters with amines (or NH_3 in (b)). In addition to H_2SO_4-C_2H_7N cluster, H_2SO_4-CH_5N and $C_4H_{11}N$ clusters were observed for H_2SO_4 trimers. NH_3 was not detected in the neutral clusters in (a). Note that due to the ionization, evaporation, and fragmentation, the amine molecule in a stable neutral H_2SO_4-amine cluster may detach during the detection by the mass spectrometer (ToF-CIMS). For instance, although $(H_2SO_4)_1(DMA)_1$ is thought to be relatively stable, the charged $(HSO_4^-)_1(DMA)_1$ is unstable and hence only HSO_4^- and $H_2SO_4NO_3^-$ were detected. In addition, although a variety of organics were detected, the concentrations of extremely low volatile organic compounds are limited (~1 order of magnitude lower compared to Finnish boreal forest). The volatility of organic compounds was estimated from their molecular formula using the volatility basis set (Donahue et al., 2011; Donahue et al., 2012). Considering the uncertainties in this estimation, the contributions of organic compounds to nucleation and the very initial steps of particle growth are thought to be minor compared to the fast H_2SO_4-amine clustering process.
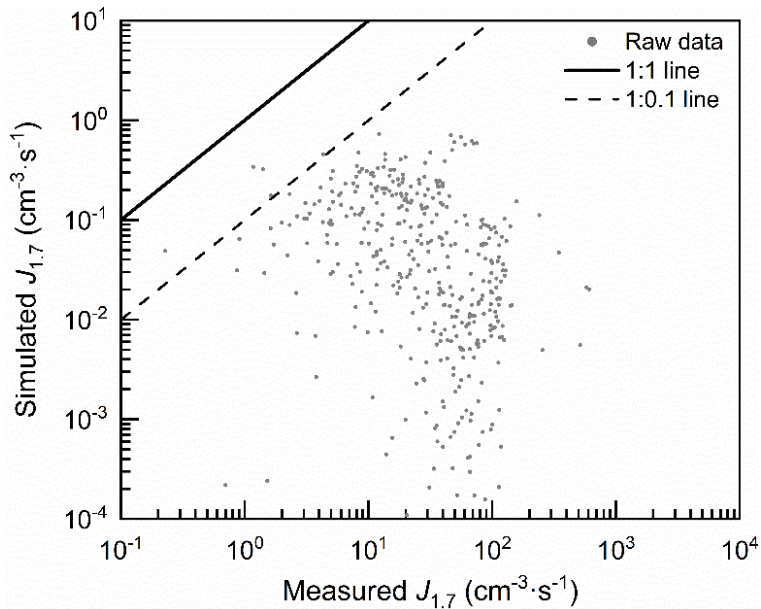
Figure S5: The measured formation rate of 1.7 nm particles, $J_{1.7}$, and the simulated $J_{1.7}$ using the organics nucleation mechanism. Only the extremely low volatile organic compounds (ELVOCs) measured by the ToF-CIMS was accounted for in the simulation. The volatility was estimated using the volatility basis set (Donahue et al., 2011; Donahue et al., 2012). The $J_{1.7}$ was simulated using the formula proposed in Kirkby et al. (2016) and ELVOCs concentration were taken as HOMs concentration. Note that the simulated $J_{1.7}$ from organics nucleation in this figure is overestimated because the CS in urban Beijing is higher than that in the CLOUD chamber, whereas the empirical formula used for this simulation does not account for the influence of CS on $J_{1.7}$. Besides, ion-induced nucleation contributes majorly the simulated $J_{1.7}$ in this figure, whereas its contribution in the polluted atmosphere is thought to be minor. Considering this overestimation and measurement uncertainties, this figure indicates the organics nucleation is insufficient to explain the high nucleation rates observed in urban Beijing.
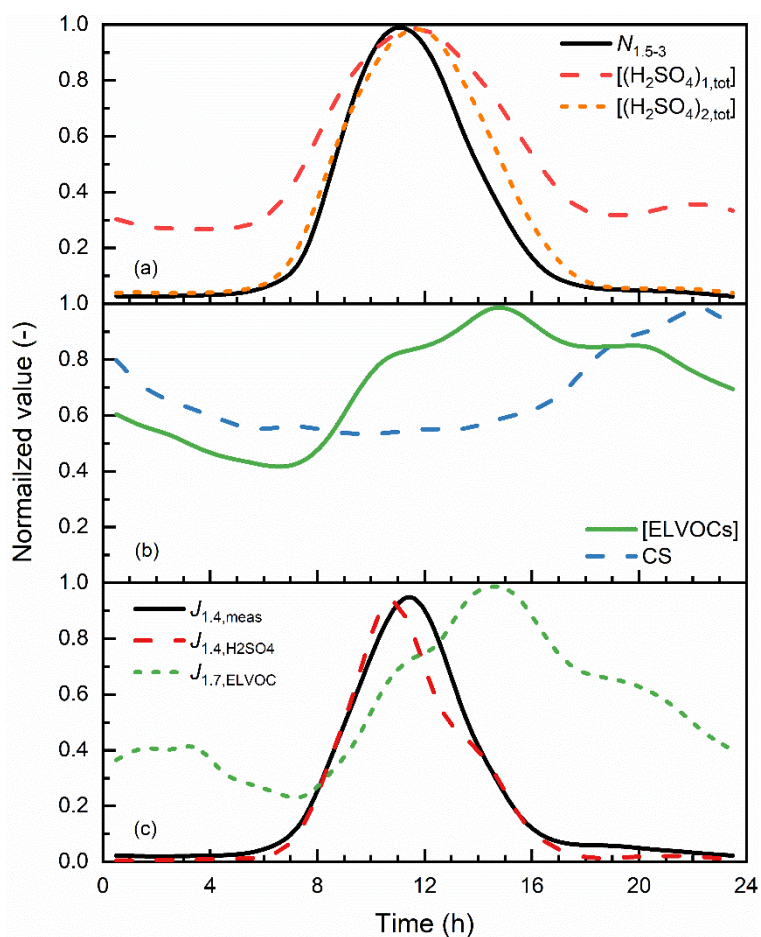
Figure S6: The diurnal variations of median (a) number concentration of particle ranging from 1.5 nm to 3 nm ($N_{1.5-3}$) H$_2$SO$_4$ monomer concentration, and H$_2$SO$_4$ dimer concentration; (b) ELVOC concentration and condensation sink (CS); (c) measured particle formation rate ($J_{1.4,\text{meas}}$) and simulated formation rates using the H$_2$SO$_4$-amine nucleation mechanism and the organics nucleation mechanism in ref. (Kirkby et al., 2016). All the variables are normalized by dividing them by their daily maximum concentration. The trend of the measured nucleation (indicated by $N_{1.5-3}$ and $J_{1.4,\text{meas}}$) is consistent with that of H$_2$SO$_4$-amine nucleation (indicated by the measured H$_2$SO$_4$ dimer concentration and the simulated $J_{1.4,\text{H2SO4}}$), whereas it is inconsistent with that of organics nucleation (indicated by the measured ELVOC concentration and the simulated $J_{1.7,\text{ELVOC}}$). Figures S5 and S6 support that organics nucleation is not the governing nucleation mechanism in urban Beijing.
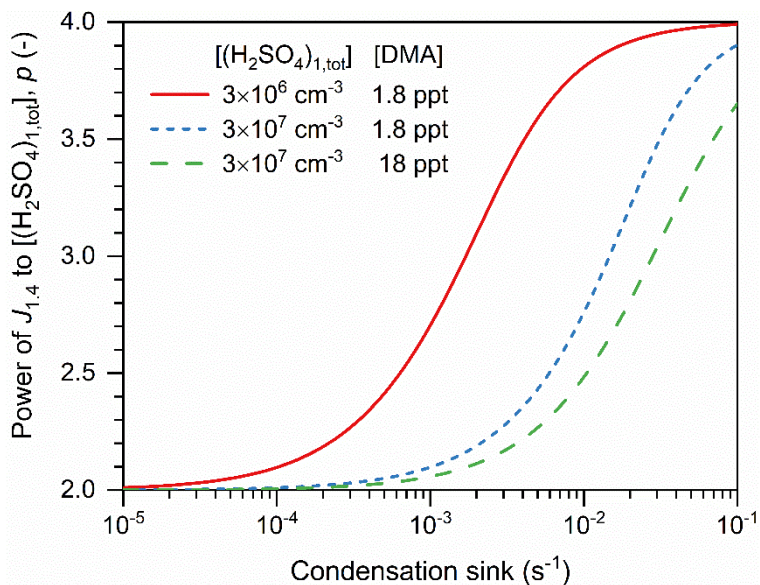
Figure S7: The power of the simulated formation rate of ~1.4 nm particles to the total concentration of H_2SO_4 monomers as a function of condensation sink. The curves are obtained at the steady-state. Under a negligible condensation sink, the formation rate of a cluster is approximately equal to its growth rate into the next cluster. Thus, the formation rate under such a condition is approximately equal to that of $(H_2SO_4)_2(DMA)_2$, which is proportional to the square of $(H_2SO_4)_{1,tot}$ concentration, i.e., $p = 2$. In contrast, the formation rate of a cluster is approximately equal to its coagulation loss rate under a high condensation sink. Given a fixed DMA concentration, Eqs. S28 indicates that $p = 4$ when the coagulation sink is the governing sink for clusters. The solid curve in this figure resembles the typical H_2SO_4 and DMA concentrations during this measurement in urban Beijing. At the typical condensation sink and temperature during new particle formation in urban Beijing, e.g., 0.017 s^{-1} and 281 K, the simulated p on the solid line is approximately 3.6.

References

Chan, T. W., and Mozurkewich, M.: Measurement of the coagulation rate constant for sulfuric acid particles as a function of particle size using tandem di!erential mobility analysis, Journal of Aerosol Science, 32, 321-339, 10.1016/S0021-8502(00)00081-1, 2001.

Donahue, N. M., Epstein, S. A., Pandis, S. N., and Robinson, A. L.: A two-dimensional volatility basis set: 1. organic-aerosol mixing thermodynamics, Atmospheric Chemistry and Physics, 11, 3303-3318, 10.5194/acp-11-3303-2011, 2011.

Donahue, N. M., Kroll, J. H., Pandis, S. N., and Robinson, A. L.: A two-dimensional volatility basis set – Part 2: Diagnostics of organic-aerosol evolution, Atmospheric Chemistry and Physics, 12, 615-634, 10.5194/acp-12-615-2012, 2012.

Halonen, R., Zapadinsky, E., Kurtén, T., Vehkamäki, H., and Reischl, B.: Rate enhancement in collisions of sulfuric acid molecules due to long-range intermolecular forces, Atmospheric Chemistry and Physics, 19, 13355-13366, 10.5194/acp-19-13355-2019, 2019.

Kirkby, J., Duplissy, J., Sengupta, K., Frege, C., Gordon, H., Williamson, C., Heinritzi, M., Simon, M., Yan, C., Almeida, J., Tröstl, J., Nieminen, T., Ortega, I. K., Wagner, R., Adamov, A., Amorim, A., Bernhammer, A.-K., Bianchi, F., Breitenlechner, M., Brilke, S., Chen, X., Craven, J., Dias, A., Ehrhart, S., Flagan, R. C., Franchin, A., Fuchs, C., Guida, R., Hakala, J., Hoyle, C. R., Jokinen, T., Junninen, H., Kangasluoma, J., Kim, J., Krapf, M., Kürten, A., Laaksonen, A., Lehtipalo, K., Makhmutov, V., Mathot, S., Molteni, U., Onnela, A., Peräkylä, O., Piel, F., Petäjä, T., Praplan, A. P., Pringle, K., Rap, A., Richards, N. A. D., Riipinen, I., Rissanen, M. P., Rondo, L., Sarnela, N., Schobesberger, S., Scott, C. E., Seinfeld, J. H., Sipilä, M., Steiner, G., Stozhkov, Y., Stratmann, F., Tomé, A., Virtanen, A., Vogel, A. L., Wagner, A. C., Wagner, P. E., Weingartner, E., Wimmer, D., Winkler, P. M., Ye, P., Zhang, X., Hansel, A., Dommen, J., Donahue, N. M., Worsnop, D. R., Baltensperger, U., Kulmala, M., Carslaw, K. S., and Curtius, J.: Ion-induced nucleation of pure biogenic particles, Nature, 533, 521-526, 10.1038/nature17953, 2016.

Kuang, C., Riipinen, I., Sihto, S. L., Kulmala, M., McCormick, A. V., and McMurry, P. H.: An improved criterion for new particle formation in diverse atmospheric environments, Atmospheric Chemistry and Physics, 10, 8469-8480, 10.5194/acp-10-8469-2010, 2010.

Kürten, A., Li, C., Bianchi, F., Curtius, J., Dias, A., Donahue, N. M., Duplissy, J., Flagan, R. C., Hakala, J., Jokinen, T., Kirkby, J., Kulmala, M., Laaksonen, A., Lehtipalo, K., Makhmutov, V., Onnela, A., Rissanen, M. P., Simon, M., Sipilä, M., Stozhkov, Y., Tröstl, J., Ye, P., and McMurry, P. H.: New particle formation in the sulfuric acid–dimethylamine–water system: reevaluation of CLOUD chamber measurements and comparison to an aerosol nucleation and growth model, Atmospheric Chemistry and Physics, 18, 845-863, 10.5194/acp-18-845-2018, 2018.

Lehtinen, K. E. J., Dal Maso, M., Kulmala, M., and Kerminen, V.-M.: Estimating nucleation rates from apparent particle formation rates and vice versa: Revised formulation of the Kerminen–Kulmala equation, Journal of Aerosol Science, 38, 988-994, 10.1016/j.jaerosci.2007.06.009, 2007.

McGrath, M. J., Olenius, T., Ortega, I. K., Loukonen, V., Paasonen, P., Kurtén, T., Kulmala, M., and Vehkamäki, H.: Atmospheric Cluster Dynamics Code: a flexible method for solution of the birth-death equations, Atmospheric Chemistry and Physics, 12, 2345-2355, 10.5194/acp-12-2345-2012, 2012.

McMurry, P. H., Fink, M., Sakurai, H., Stolzenburg, M. R., Mauldin, R. L., Smith, J., Eisele, F., Moore, K., Sjostedt, S., Tanner, D., Huey, L. G., Nowak, J. B., Edgerton, E., and Voisin, D.: A criterion for new particle formation in the sulfur-rich Atlanta atmosphere, Journal of Geophysical Research, 110, D22S02, 10.1029/2005jd005901, 2005.

Myllys, N., Kubečka, J., Besel, V., Alfaouri, D., Olenius, T., Smith, J. N., and Passananti, M.: Role of base strength, cluster structure and charge in sulfuric-acid-driven particle formation, Atmospheric Chemistry and Physics, 19, 9753-9768, 10.5194/acp-19-9753-2019, 2019.

Ortega, I. K., Kupiainen, O., Kurtén, T., Olenius, T., Wilkman, O., McGrath, M. J., Loukonen, V., and Vehkamäki, H.: From quantum chemical formation free energies to evaporation rates, Atmospheric Chemistry and Physics, 12, 225-235, 10.5194/acp-12-225-2012, 2012.

Stolzenburg, D., Simon, M., Ranjithkumar, A., Kürten, A., Lehtipalo, K., Gordon, H., Nieminen, T., Pichelstorfer, L., He, X.-

C., Brilke, S., Xiao, M., Amorim, A., Baalbaki, R., Baccarini, A., Beck, L., Bräkling, S., Caudillo Murillo, L., Chen, D., Chu, B., Dada, L., Dias, A., Dommen, J., Duplissy, J., El Haddad, I., Finkenzeller, H., Fischer, L., Gonzalez Carracedo, L., Heinritzi, M., Kim, C., Koenig, T. K., Kong, W., Lamkaddam, H., Lee, C. P., Leiminger, M., Li, Z., Makhmutov, V., Manninen, H. E., Marie, G., Marten, R., Müller, T., Nie, W., Partoll, E., Petäjä, T., Pfeifer, J., Philippov, M., Rissanen, M. P., Rörup, B., Schobesberger, S., Schuchmann, S., Shen, J., Sipilä, M., Steiner, G., Stozhkov, Y., Tauber, C., Tham, Y. J., Tomé, A., Vazquez-Pufleau, M., Wagner, A. C., Wang, M., Wang, Y., Weber, S. K., Wimmer, D., Wlasits, P. J., Wu, Y., Ye, Q., Zauner-Wieczorek, M., Baltensperger, U., Carslaw, K. S., Curtius, J., Donahue, N. M., Flagan, R. C., Hansel, A., Kulmala, M., Volkamer, R., Kirkby, J., and Winkler, P. M.: Enhanced growth rate of atmospheric particles from sulfuric acid, Atmospheric Chemistry and Physics Discussions, in review, 10.5194/acp-2019-755, 2019.

Thomas, J. M., He, S., Larriba-Andaluz, C., DePalma, J. W., Johnston, M. V., and Hogan, C. J., Jr.: Ion mobility spectrometry-mass spectrometry examination of the structures, stabilities, and extents of hydration of dimethylamine-sulfuric acid clusters, Physical Chemistry Chemical Physics, 18, 22962-22972, 10.1039/c6cp03432b, 2016.